

# Residual stresses couple microscopic and macroscopic scales

Sebastian Steinhäuser,<sup>1,2</sup> Timm Treskatis,<sup>3</sup> Stefan Turek,<sup>3</sup> and Thomas Voigtmann<sup>1,2</sup>

<sup>1</sup>*Institut für Materialphysik im Weltraum, Deutsches Zentrum für Luft- und Raumfahrt (DLR) e.V., 51170 Köln, Germany*  
<sup>2</sup>*Heinrich-Heine-Universität Düsseldorf, Universitätsstraße 1, 40225 Düsseldorf, Germany*

<sup>3</sup>*Institut für Angewandte Mathematik (LS3), Technische Universität Dortmund, Vogelpothsweg 87, 44227 Dortmund, Germany*  
(Dated: July 25, 2023)

We show how residual stresses emerge in a visco-elastic material as a signature of its past flow history, through an interplay between flow-modified microscopic relaxation and macroscopic features of the flow. Long-lasting temporal-history dependence of the microscopic dynamics and nonlinear rheology are incorporated through the mode-coupling theory of the glass transition (MCT). The theory’s integral constitutive equation (ICE) is coupled to continuum mechanics in a finite-element method (FEM) scheme that tracks the flow history through the Finger tensor. The method is suitable for a calculation of residual stresses from a “first-principles” starting point following well-understood approximations. As an example, we calculate within a schematic version of MCT the stress-induced optical birefringence pattern of an amorphous solid cast into the shape of a slab with a cylindrical obstacle and demonstrate how FEM-MCT can predict the dependence of material properties on the material’s processing history.

Materials that flow carry stresses, and once such a material solidifies, some of those stresses can remain in the solid as flow-induced residual stresses. While the textbook elastic solid is assumed to be stressed only if strained, the possibility of internal stresses has been discussed theoretically since at least the 1930’s [1]. All continuum mechanics requires, is that the stress tensor  $\sigma$  inside the material is self-equilibrated,  $\nabla \cdot \sigma = 0$ , which in general allows non-zero stresses at rest.

Residual stresses are now recognized as a major factor controlling the mechanical [2, 3] and optical [4–7] performance of materials and composites [8]. They arise from rapid solidification, through chemical means, or from spatial variations in the material coefficients. Spectacular demonstrations of their effect go back to exploding glass droplets by Prince Rupert in the 1660’s [9–11], and perhaps [12] to the images produced by “magic mirrors” (透光镜) of the Western Han dynasty around 200 B.C. [13, 14]. The controlled use of residual stresses allows to produce improved materials [15], such as scratch-resistant smartphone covers or safety glasses. The stability of thin films and coatings, produced from a strongly flowing state, depends on control of residual stresses [16]; in micro-electromechanical systems (MEMS) they have decisive influence on the device’s function [17]. In turn, coatings allow to control residual stresses, e.g., in additively manufactured biocompatible implants [18]. Residual stresses play an important factor in maintaining homeostatic states in living tissues [19–24]. Finally, additive manufacturing (AM) has re-emphasized the role of residual stresses in determining the mechanical properties and failure behavior of the final piece [25–27]. Despite their ubiquitous nature and importance, residual stresses remain hard to measure [28–31], which necessitates improved models.

We aim to explain residual stresses in amorphous materials, in particular colloidal materials [32, 33] after ces-

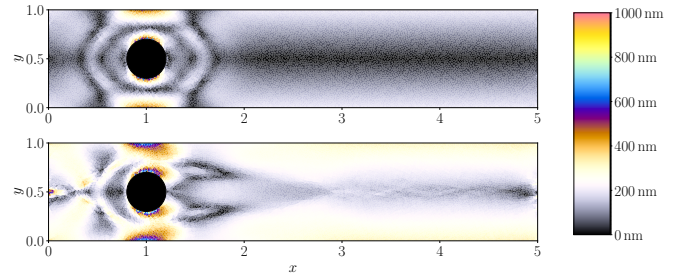


FIG. 1. Residual-stress induced birefringence in a 5:1 rectangular (periodic) channel with a circular obstacle, after cessation of a pressure-driven flow with pressure drops (a)  $\Delta p/G_0 = 1$ , (b)  $\Delta p/G_0 = 10$ . Colors represent optical path lengths for white-light illumination (as indicated by the color bar) assuming sample thickness  $h$  and stress-optical coefficient  $C$  such that  $CG_0h = 80 \mu\text{m}$  respectively  $800 \mu\text{m}$ , following a standard CIE color model (see text for details).

sation of flow, in a theoretical framework that is founded in microscopic principles: the combination of mode-coupling theory of the glass transition (MCT) with the finite-element method (FEM). The FEM-MCT model predicts the appearance of spatial patterns of residual stresses in an amorphous solids that depend on both the flow history and geometry. For example, the morphology of stresses remaining around a cylindrical obstacle in a channel depends crucially on the pressure gradient that was used to drive the flow before it came to rest (Fig. 1). It reveals an interesting interplay between macroscopic symmetries of the flow, and microscopic relaxation response, *i.e.*, a true *multi-scale* phenomenon: whether and how many residual stresses remain, depends on how the microscopic relaxation is modified by, and influences the, macroscopic flow.

Predicting flow-induced residual stresses in glassy materials from first principles is not a simple task: they remain because the structural relaxation dynamics of the

material becomes extremely slow, and moreover the microscopic relaxation mechanisms are strongly influenced by the macroscopic flow conditions (rendering it a problem of nonlinear rheology). The phenomenon is thus intrinsically a non-equilibrium, non-linear response one: it is the relaxation from a flowing to the quiescent state that gets “stuck” in a stressed out-of-equilibrium state. This also implies that residual stresses depend on the past processing history of a material. Thus, a description of the material in its final state is incomplete, and one requires a model that includes the complete flow history in its constitutive equation. There is no separation of time scales between the microscopic relaxation and the macroscopic flow. This is a much more complicated situation than for example the modeling of thermal residual stresses [34–38].

The accepted theory of macroscopic flow is formulated through the Navier-Stokes equations for the mass density  $\rho(t, \vec{x})$  and the flow velocity  $\vec{v}(t, \vec{x})$ ,

$$\rho \frac{D}{Dt} \vec{v} = -\vec{\nabla} p + \vec{\nabla} \cdot \boldsymbol{\sigma} \quad (1)$$

where  $D/Dt = \partial_t + \vec{v} \cdot \vec{\nabla}$  is the advected derivative and  $p$  is the pressure applied to the system.

The stress tensor  $\boldsymbol{\sigma}$  encodes the dissipative terms that arise in the coarse-graining implicit in Eq. (1). They need to be described by a material law, in the form of a constitutive equation (CE) that links the stress tensor back to the fields, most notably to suitably frame-invariant combinations of the velocity gradients  $\boldsymbol{\kappa} = \vec{\nabla} \vec{v}$ . Most CE used in the literature are empirical, encoding the microscopic details of a material in a few ad-hoc parameters. Here, we will follow an approach that rests on a microscopic theory for  $\boldsymbol{\sigma}$  for glass-forming fluids. It will be useful to split  $\boldsymbol{\sigma} = \boldsymbol{\sigma}_N + \boldsymbol{\sigma}_P$ , where  $\boldsymbol{\sigma}_N = \eta_\infty (\boldsymbol{\kappa} + \boldsymbol{\kappa}^T)$  describes a Newtonian background viscosity of the fluid.

For slow structural relaxation in glass-forming fluids, a successful microscopic theory is the MCT, specifically its extension to (colloidal) rheology [39–42]. Using the integration through transients (ITT), a general non-equilibrium statistical-physics framework, one derives a material law of the form

$$\boldsymbol{\sigma}_P(t) = \int_{-\infty}^t \mathbb{G}(t, t', [\mathbf{B}]) : [-\partial_{t'} \mathbf{B}_{tt'}] dt', \quad (2)$$

where the flow enters through the Finger tensor  $\mathbf{B}_{tt'}$ , the rotation-invariant measure of deformations occurring between time  $t'$  and  $t \geq t'$ . Standard continuum-mechanics arguments imply [43]

$$\vec{\nabla} \mathbf{B}_{tt'} = \frac{D}{Dt} \mathbf{B}_{tt'} - \boldsymbol{\kappa}_t \cdot \mathbf{B}_{tt'} - \mathbf{B}_{tt'} \cdot \boldsymbol{\kappa}_t^T = \mathbf{0}. \quad (3)$$

The generalized non-linear-response shear modulus  $\mathbb{G}$  (a fourth-rank tensor) encodes the microscopic stress relaxation and bears a functional dependence on  $\mathbf{B}$  representing the flow history. Equation (2) is the general form

expected from statistical physics, as it describes the time-delayed response of a system to a past perturbation. In rheological terms, it is an integral constitutive equation (ICE) that—in contrast to most empirical laws—cannot be rewritten as a differential equation (because of the functional dependence of  $\mathbb{G}$  on the flow). CE are not in general partial differential equations, because they are not local conservation laws in contrast to the fundamental field-theory laws. This poses a major complication for the numerical approach together with the FEM, but it also encodes physically relevant flow-history phenomena, such as those giving rise to residual stresses.

ITT provides a microscopic expression for  $\mathbb{G}$  upon which MCT constructs an approximate CE derived from first principles, and predicts the appearance of residual stresses [32]. It works under the assumption that the flow is slowly varying in space and that stress relaxation is dominated by the relaxation of density fluctuations on the length scale of interparticle separation. We consider low-Reynolds-number flow on long time scales; for this reason the formulation of MCT for colloidal suspensions is sufficient. In order to highlight the qualitative features predicted by MCT, we proceed with an established schematic model [44] that approximates the shear modulus by an isotropic form,  $G_{ijkl}(t, t', [\mathbf{B}]) = \delta_{ik} \delta_{jl} G(t, t', [\mathbf{B}])$ . Further approximations replacing  $G$  by a simple decay function,  $G(t, t') \approx G_\infty \exp[-(t - t')/\tau]$ , say, would recover from Eq. (2) the upper-convected Maxwell model for  $\boldsymbol{\sigma}_P$ , or equivalently, the Oldroyd B model for  $\boldsymbol{\sigma}$ . This type of model misses two ingredients to predict history-dependent residual stresses, that MCT adds:  $G$  is not time-translational invariant, and it needs to depend on the flow history itself.

Technically, schematic MCT encodes time-delayed response in a non-Markovian model for the dominant density-relaxation mode  $\phi(t, t')$ . Neglecting macroscopic gradients in this dynamics [45],  $\vec{v} \cdot \vec{\nabla} \phi \approx 0$ , we set  $G(t, t', [\mathbf{B}], \vec{x}) \approx G_0 \phi^2(t, t', [\mathbf{B}], \vec{x})$  and [44]

$$\tau_0 \partial_t \phi(t, t', \vec{x}) + \phi(t, t', \vec{x}) \quad (4a)$$

$$+ \int_{t'}^t m(t, t'', t', \vec{x}) \partial_{t''} \phi(t'', t', \vec{x}) dt'' = 0,$$

$$m(t, t'', t') = h_{tt''}[\mathbf{B}] h_{t't'}[\mathbf{B}] (v_1 \phi(t, t'') + v_2 \phi^2(t, t'')), \quad (4b)$$

dropping notation of  $\vec{x}$ - and  $\mathbf{B}$ -dependence as convenient. The latter comes in through the memory-loss functions,  $h_{tt'}[\mathbf{B}] = 1/(1 + \text{tr}(\mathbf{B}_{tt'} - \mathbf{1})/\gamma_c^2)$  that describe decorrelation of microscopic density fluctuations by flow advection. The parameter  $\gamma_c = 1/10$  fixes a strain scale to connect to microscopic units.

The core of MCT is the approximation Eq. (4b). In the schematic model,  $(v_1, v_2)$  play the role of the coupling coefficients that within the full theory are given by the equilibrium static structure functions of the fluid. At a certain coupling strength (*e.g.*, driven by density or tem-

perature), the solutions of Eq. (4) turn *glassy*: there is a set of critical points  $(v_1^c, v_2^c)$  separating fluid-like solutions characterized by  $\lim_{t \rightarrow \infty} \phi(t, t', [\mathbf{B} = 0]) = 0$  from glass-like ones,  $\lim_{t \rightarrow \infty} \phi(t, t', [\mathbf{B} = 0]) = f > 0$ . Setting  $(v_1, v_2) = (v_1^c + \epsilon/(\sqrt{2} - 1), v_2^c)$  with  $v_2^c = 2$  and  $v_1^c = 2(\sqrt{2} - 1)$  ensures the asymptotic features of the model to match that found by fully microscopic calculations for typical colloidal suspensions [44].

We fix  $\epsilon = 1/100$ ; this implies that we study a material that is glassy at rest, but has a yield stress of  $\sigma_y = G_\infty \gamma_c$  with  $G_\infty = G_0 f^2 \approx G_0/10$ , and will be fluidized locally when the stress is above this value. The model predicts shear thinning, common empirical tensorial yield criteria [44], and residual stresses upon instantaneous cessation of simple-shear flow [32, 46].

The results shown here have been obtained by a combined numerical scheme that uses the finite-element method (FEM) augmented with a fully nonstationary MCT solver (adapted from Ref. [47]). A Marchuk-Yanenko splitting disentangles the calculation of  $(\vec{v}, p)$  [Eq. (1)] from that of  $(\mathbf{B}, G)$  [Eqs. (2)–(4)] into separate iterative time steps. All time-derivatives are discretized with a simple implicit Euler scheme. For each  $t' < t$  the Finger tensors are approximated as piecewise constant in space and determined from Eq. (3). The stresses are then evaluated following the solution of Eqs. (4). Since the relaxation functions extend far back in time, but also become slowly varying, a pseudo-logarithmic grid in  $t - t'$  is employed. The updated stress contribution  $\sigma_P$  then enters Eq. (1), which is solved at each time step with a standard  $P_2 - P_0$  finite-element scheme, using second-order continuous Lagrange elements (CG2) for the velocity, and discontinuous zeroth-order elements (DG0) for stress and pressure, ensuring correct cellwise mass and momentum conservation. The entire code is implemented in the programming language Python, using the package FEniCS (version 2019.2) [48, 49] for the solution of the discretized Navier-Stokes equations, employing the MUMPS LU solver. In comparison to previous attempts of integrating MCT with continuum mechanics based on the Lattice-Boltzmann (LB) technique [50], FEM offers a more straight-forward approach to deal with non-Newtonian flows in complex geometries and using non-uniform meshes.

We consider two-dimensional incompressible ( $\vec{\nabla} \cdot \vec{v} = 0$ ) flow in an infinite rectangular channel (height  $H$ , periodicity  $L = 5H$  along the  $x$ -direction) that is initially driven by a pressure gradient,  $\vec{\nabla} p(t) = -(\Delta p/L)\vec{e}_x$  for  $0 < t < t_{\text{off}}$ . Periodic boundary conditions are applied in the  $x$ -direction, no-slip boundary conditions on the walls perpendicular to the  $y$ -direction. The pressure gradient is removed,  $\vec{\nabla} p(t) = 0$ , for  $t > t_{\text{off}}$ . To break the trivial  $x$ -translation symmetry of the problem, a circular obstacle (radius  $0.2H$ , no-slip b.c.) is placed centered in the channel at  $(x_0, y_0) = (1, 0.5)H$ .

Setting  $G_0 = 1$ ,  $\eta_\infty = 1$ , and  $\tau_0 = 1$  fixes the remain-

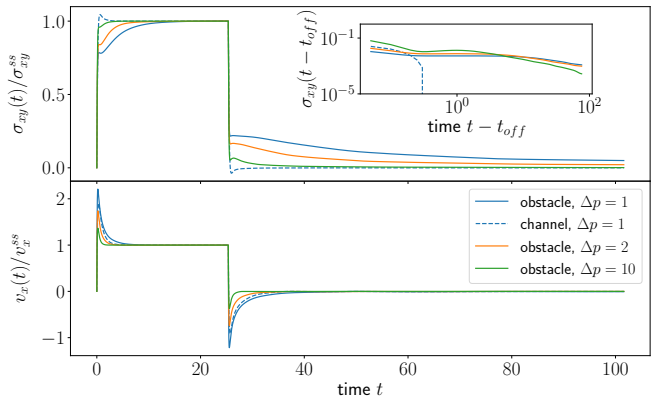


FIG. 2. Shear stress  $\sigma_{xy}(t)$  and velocity  $v_x(t)$  as a function of time in the 5:1 rectangular channel with cylindrical obstacle (solid lines), for different initial driving pressures  $\Delta p/G_0$  as indicated (active for  $0 < t < t_{\text{off}} = 25.470$ ). The inset provides a logarithmic zoom of the stress decay. Dashed lines correspond to a channel without obstacle.

ing units. The time step for the numerical solution is  $dt = 0.05$ , on a grid with 128 mesh cells across its diameter. With these parameters, a single run (2032 timesteps) takes around 10 days utilizing 24 cores of a dual Xeon E5-2650v4 workstation and around 45 GB of memory.

We prepare initial flowing states by applying a constant pressure gradient to the stress-free material at rest; the driving force is switched off instantaneously at  $t_{\text{off}} = 25.470$ . The velocity initially increases towards the stationary state through a distinctive overshoot typical for the startup flow of viscoelastic fluids [50]; the stresses concomitantly increase towards their stationary values on a somewhat longer time scale (Fig. 2).

After removal of the pressure gradient, the velocity displays a pronounced undershoot before relaxing towards zero. This can be rationalized as another viscoelastic effect [50]: the presence of stresses causes the fluid to be driven in the direction opposite of the initial flow direction, until the stresses have sufficiently relaxed.

Crucially, we observe the shear stress  $\sigma_{xy}(t)$  to completely relax in the channel without obstacle (dashed line in Fig. 2), while in the presence of the obstacle, the velocity back-leash is much less pronounced, and finite shear stresses remain even for times where the velocity has already decayed to zero. These are geometry-dependent residual stresses. The difference arises from the coupling of the macroscopic deformation gradients into the microscopic relaxation, Eqs. (4). The macroscopic momentum balance at rest,  $\vec{\nabla} \cdot \boldsymbol{\sigma} = 0$ , implies  $\partial_y \sigma_{xy} = -\partial_x \sigma_{xx}$ , and thus any residual shear stress arising from a flow that is translational invariant along the  $x$ -direction, needs to obey  $\sigma_{xy}(y) = \text{const}$ . For homogeneous simple shear between parallel plates, Eqs. (4) in the glass ( $\epsilon \geq 0$ ) predict a finite residual shear stress  $\sigma_{xy}(t \rightarrow \infty) = \sigma_\infty > 0$  [32, 46], automatically com-

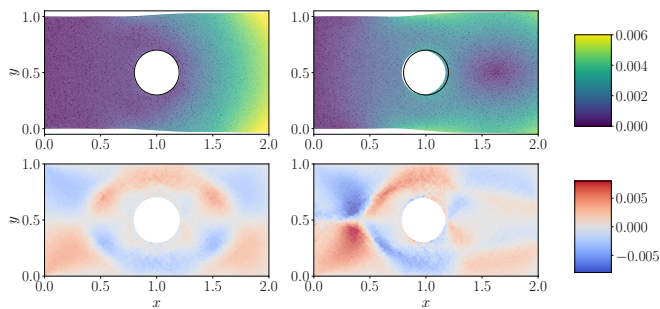


FIG. 3. Top: Eigenstrain balancing the residual stresses after cutting a section of width  $\Delta x = 2$  from the channel, for initial pressure drop  $\Delta p/G_0 = 1$  (left) and  $\Delta p/G_0 = 10$  (right). The magnitude is shown as color, the deformation of the sample is shown amplified by a factor 10 respectively 100. Bottom: corresponding relaxed residual shear stress  $\hat{\sigma}_{xy}$  (result for  $\Delta p/G_0 = 10$  left magnified by a factor 10).

patible with  $\vec{\nabla} \cdot \boldsymbol{\sigma} = 0$ . The  $x$ -translationally invariant channel flow imposes  $\sigma_{xy}(y = 0) = 0$  by symmetry, so that here  $\sigma_\infty = 0$  is the only solution compatible with the macroscopic momentum balance. If however the translational symmetry is broken (e.g., by the obstacle), non-zero residual shear stresses become permissible again. This is the non-trivial solution obtained from FEM-MCT.

To connect to typical measurements, Fig. 1 presents stress patterns as if observed for an optically stress-induced birefringent medium between crossed circular polarizers. This polarimeter setup is commonly used as a non-destructive method to assess internal stresses in optically transparent media [51]. It rests on the stress-optical effect: otherwise non-birefringent materials become optically birefringent in response to mechanical stress. To first order, there holds Maxwell’s stress-optical law [52],  $\Delta n = n_o - n_e = C(\sigma_1 - \sigma_2)$ , where  $\sigma_{1,2}$  are the stress eigenvalues in the plane perpendicular to the propagation of light, and  $n_{o,e}$  are the refractive indices along the optical axes defined by the corresponding stress eigenvectors.  $C$  is called the stress-optical coefficient. Assuming a slab of material whose properties are invariant along the light-propagation direction (taken to be along  $z$ ), a textbook calculation shows that the transmitted light intensity when placing the sample between two circular polarizers, is  $I(\lambda, \delta) = I_0(\lambda) \cos(\delta/2)^2$ , where  $\delta = (2\pi z/\lambda)\Delta n$  is the (stress-dependent) optical retardation. If we assume illumination by a white-light source ( $I_0$  constant across the visible spectrum  $\lambda \in [360, 830]$ nm), a colorful transmission spectrum will be recorded by the observer. This spectrum  $I(\lambda, \delta)$  can be converted to empirical RGB values of colors as perceived by the human eye [53]. This is the color bar used in Fig. 1.

To illustrate the effect of the residual stresses on the mechanical properties of the final material, let us consider the glass as a linear-elastic material with stress tensor

$\boldsymbol{\sigma} = \boldsymbol{\sigma}_{\text{res}} + \hat{\boldsymbol{\sigma}}(\boldsymbol{\varepsilon})$ , composed of a residual stress and a strain-dependent elastic stress. The deformation field  $\vec{u}$  in the material’s bulk volume  $\Omega$  solves

$$\vec{\nabla} \cdot [\hat{\boldsymbol{\sigma}} + \boldsymbol{\sigma}_{\text{res}}] = 0 \quad \text{in } \Omega, \quad (5a)$$

$$\hat{\boldsymbol{\sigma}} = \lambda(\text{tr } \boldsymbol{\varepsilon})\mathbf{1} + 2\mu\boldsymbol{\varepsilon}, \quad (5b)$$

$$\boldsymbol{\varepsilon} = (\vec{\nabla}\vec{u} + (\vec{\nabla}\vec{u})^T)/2. \quad (5c)$$

Here,  $\boldsymbol{\sigma}_{\text{res}} = \boldsymbol{\sigma}_P(t \rightarrow \infty)$  is approximated by the final-time stress tensor obtained from FEM-MCT. The set of Eqs. (5) is solved by a standard FEM simulation with  $\mu = G_0$  and  $\lambda = 1.5G_0$ , using CG1 elements for the displacement field. A truly self-equilibrated stress,  $\vec{\nabla} \cdot \boldsymbol{\sigma}_{\text{res}} = 0$  does not enter linear elasticity at all. However, this hinges on the boundary conditions: for  $\boldsymbol{\sigma}_{\text{res}}$  generated by the channel flow inside fixed walls, these correspond to  $\vec{u} = 0$  on  $\partial\Omega$ . For the sake of demonstration, let us “cut” the solid from its casting shape, i.e., change to free boundary conditions,  $\boldsymbol{\sigma} \cdot \vec{n} = 0$  on  $\partial\Omega$  except on vertical walls at  $x \in \{0, 2H\}$  (where  $\vec{u} = 0$  is imposed). It implies  $\hat{\boldsymbol{\sigma}} \cdot \vec{n} = -\boldsymbol{\sigma}_{\text{res}} \cdot \vec{n}$  and an ensuing non-trivial deformation field  $\vec{u}$  in  $\Omega$ . These eigenstrains caused by the residual stresses are shown in Fig. 3(a,b) for the two different residual-stress levels; the comparison brings out that they are indeed noticeably different, i.e., the material has different elastic properties due to its different past-flow history. The eigenstrains relax some of these stresses, but still, relaxed residual stresses remain, as shown in Fig. 3(c,d).

Both the unrelaxed (Fig. 1) and relaxed (Fig. 3) stresses show an interesting viscoelastic symmetry-breaking effect: Since the stationary Stokes-flow solution for a Newtonian fluid is time-reversal symmetric (the basis of the famous no-swimming theorem at low Reynolds number [54]), the corresponding flow patterns obey an inflection symmetry around the obstacle. Our results for small  $\Delta p/G_0$  demonstrate this. But for large  $\Delta p/G_0$ , viscoelastic terms from the ICE break this symmetry, even in zero-Reynolds-number flow. It appears that the residual stresses exhibit the pattern of “viscoelastic turbulence” [55–57] even though typically shear thinning is observed to suppress the effect in stationary flow [45, 58].

To conclude, we presented predictions of residual-stress patterns emerging in non-trivial flow geometry, based on a microscopic theory of the flow of glass-forming fluids, the MCT, combined with FEM simulations that allow to bridge from the microscopic to the macroscopic scale. We see this as a first conceptual step towards a scale-bridging approach modeling a material’s property through its entire processing history.

The cessation of pressure-driven channel flows reveals an intriguing coupling of microscopic and macroscopic scales: While MCT in principle allows for residual stresses simply due to the infinite microscopic structural relaxation time in the ideal glass, continuum mechanics enforces those stresses to be macroscopically self-

equilibrated, i.e.,  $\vec{\nabla} \cdot \boldsymbol{\sigma} = 0$  at rest. Through this, the macroscopic symmetries and boundary conditions enter the microscopic relaxation dynamics and change it qualitatively.

This work has been funded by the Deutsche Forschungsgemeinschaft (DFG, German Research Foundation) – project number 431117597.

- 
- [1] H. Reißner, *Z. Angew. Math. Mech.* **11**, 1 (1931).
- [2] P. J. Withers, *Rep. Prog. Phys.* **70**, 2211 (2007).
- [3] S. Hirobe, K. Imakita, H. Aizawa, Y. Kato, S. Urata, and K. Oguni, *Phys. Rev. Lett.* **127**, 064301 (2021).
- [4] D. J. Wissucheck, C. W. Ponader, and J. J. Price, in *Optical Fiber Reliability and Testing*, Proceedings of SPIE, Vol. 3848, edited by M. J. Matthewson (SPIE, 1999) pp. 34–43.
- [5] A. D. Yablon, *IEEE J. Quantum Electr.* **10**, 300 (2004).
- [6] A. Y. Yi, B. Tao, F. Klocke, O. Dambon, and F. Wang, *Proc. Eng.* **19**, 402 (2011).
- [7] B. McMillen, C. Athanasiou, and Y. Bellouard, *Opt. Express* **24**, 27239 (2016).
- [8] P. P. Parlevliet, H. E. N. Bersee, and A. Beukers, *Composites A* **37**, 1847 (2006); **38**, 651 (2007).
- [9] H. Aben, J. Anton, M. Öis, K. Viswanathan, S. Chandrasekar, and M. M. Chaudhri, *Appl. Phys. Lett.* **109**, 231903 (2016).
- [10] L. Brodsley, C. Frank, and J. W. Steeds, *Notes Rec. R. Soc. Lond.* **41**, 1 (1986).
- [11] S. Chandrasekar and M. M. Chaudhri, *Philos. Mag. B* **70**, 1195 (1994).
- [12] M. V. Berry, *Eur. J. Phys.* **27**, 109 (2006).
- [13] J. K. Murray and S. E. Cahill, *Chinese Science* **8**, 1 (1987).
- [14] Y. lai Yan, *Physics Teacher* **30**, 341 (1992).
- [15] Y. Zhang, W. H. Wang, and A. L. Greer, *Nature Materials* **5**, 857 (2006).
- [16] G. Reiter, M. Hamieh, P. Damman, S. Sclavons, S. Gabriele, T. Vilmin, and E. Raphaël, *Nature Materials* **4**, 754 (2005).
- [17] M. Schlögl, J. Weißenbach, M. Schneider, and U. Schmid, *Sensors & Actuators A* **349**, 114067 (2023).
- [18] M. Hein, *Crystals* **12**, 1190 (2022).
- [19] Y. C. Fung, *Biomechanics: Motion, flow, stress, and growth* (Springer, New York, 1990).
- [20] Y. Lanir, *J. Biomech. Eng.* **131**, 044506 (2009).
- [21] Y. Lanir, *J. Elast.* **129**, 7 (2017).
- [22] J. A. Peña, M. A. Martínez, and E. Peña, *J. Mech. Beh. Biomed. Mat.* **50**, 55 (2015).
- [23] P. Ciarletta, M. Destrade, and A. L. Gower, *Sci. Rep.* **6**, 24390 (2016).
- [24] T. Sigaeva, G. Sommer, G. A. Holzapfel, and E. S. Di Martino, *J. R. Soc. Interface* **16**, 20190029 (2019).
- [25] P. Mercelis and J.-P. Kruth, *Rapid Prototyping Journal* **12**, 254 (2006).
- [26] E. A. Patterson, J. Lambros, R. Magana-Carranza, and C. J. Sutcliffe, *Int. J. Adv. Manuf. Technol.* **123**, 1845 (2022).
- [27] W. Chen, T. Voisin, Y. Zhang, J.-B. Forien, C. M. Spadaccini, D. L. McDowell, T. Zhu, and Y. Morris Wang, *Nature Commun.* **10**, 4338 (2019).
- [28] J. P. Withers and H. K. D. H. Bhadeshia, *Mater. Sci. Technol.* **17**, 355 (2001).
- [29] J. P. Withers and H. K. D. H. Bhadeshia, *Mater. Sci. Technol.* **17**, 366 (2001).
- [30] G. S. Schajer, ed., *Practical Residual Stress Measurement Methods* (Wiley & Sons, West Sussex, 2013).
- [31] J. Guo, H. Fu, B. Pan, and R. Kang, *Chinese J. Aeronautics* **34**, 54 (2021).
- [32] M. Ballauff, J. M. Brader, S. U. Egelhaaf, M. Fuchs, J. Horbach, N. Koumakis, M. Krüger, M. Laurati, K. J. Mutch, G. Petekidis, M. Siebenbürger, T. Voigtmann, and J. Zausch, *Phys. Rev. Lett.* **110**, 215701 (2013).
- [33] L. Mohan, R. T. Bonnecaze, and M. Cloitre, *Phys. Rev. Lett.* **111**, 268301 (2013).
- [34] H. L. Wei, T. Mukherjee, W. Zhang, J. S. Zuback, G. L. Knapp, A. De, and T. DebRoy, *Prog. Mater. Sci.* **116**, 100703 (2021).
- [35] Y. Chen, A. Y. Yi, L. Su, F. Klocke, and G. Pongs, *J. Manuf. Sci. Engin.* **130**, 051012 (2008).
- [36] M. Strantza, R. K. Ganeriwala, B. Clausen, T. Q. Phan, L. E. Levine, D. Pagan, W. E. King, N. E. Hodge, and D. W. Brown, *Mater. Letters* **231**, 221 (2018).
- [37] F. Chen and W. Yan, *Materials and Design* **196**, 109185 (2020).
- [38] N. Grilli, D. Hu, D. Yushu, F. Chen, and W. Yan, *Comput. Mech.* **69**, 825 (2021).
- [39] M. Fuchs and M. E. Cates, *Phys. Rev. Lett.* **89**, 248304 (2002).
- [40] J. M. Brader, T. Voigtmann, M. E. Cates, and M. Fuchs, *Phys. Rev. Lett.* **98**, 058301 (2007).
- [41] J. M. Brader, M. E. Cates, and M. Fuchs, *Phys. Rev. Lett.* **101**, 138301 (2008).
- [42] M. Fuchs and M. E. Cates, *J. Rheol.* **53**, 957 (2009).
- [43] M. E. Gurtin, E. Fried, and L. Anand, *The Mechanics and Thermodynamics of Continua* (Cambridge University Press, Cambridge, 2009).
- [44] J. M. Brader, T. Voigtmann, M. Fuchs, R. G. Larson, and M. E. Cates, *Proc. Natl. Acad. Sci. USA* **106**, 15186 (2009).
- [45] A. Nicolas and M. Fuchs, *J. Non-Newt. Fluid Mech.* **228**, 64 (2016).
- [46] S. Fritschi, M. Fuchs, and T. Voigtmann, *Soft Matter* **10**, 4822 (2014).
- [47] T. Voigtmann, J. M. Brader, M. Fuchs, and M. E. Cates, *Soft Matter* **8**, 4244 (2012).
- [48] A. Logg, K.-A. Mardal, and G. N. Wells, eds., *Automated Solution of Differential Equations by the Finite Element Method*, Lecture Notes in Computational Science and Engineering, Vol. 84 (Springer, Berlin, Germany, 2012).
- [49] The fenics project, <https://fenicsproject.org/>.
- [50] S. Papenkort and T. Voigtmann, *J. Chem. Phys.* **140**, 164507 (2014); **143**, 044512 (2015); **143**, 204502 (2015).
- [51] D. V. Nelson, *J. Phys.: Photonics* **3**, 044003 (2021).
- [52] J. C. Maxwell, *J. Trans. Roy. Soc. Edinb.* **20**, 87 (1853).
- [53] B. E. Sørensen, *Eur. J. Mineral.* **25**, 5 (2013).
- [54] E. M. Purcell, *Am. J. Phys.* **45**, 3 (1977).
- [55] A. Groisman and V. Steinberg, *Nature (London)* **405**, 53 (2000).
- [56] R. G. Larson, *Nature (London)* **405**, 27 (2000).
- [57] A. N. Morozov and W. van Saarloos, *Phys. Rep.* **447**, 112 (2007).
- [58] L. Casanellas, M. A. Alves, R. J. Poole, S. Lerouge, and A. Lindner, *Soft Matter* **12**, 6167 (2016).